Nanoscale

Accepted Manuscript

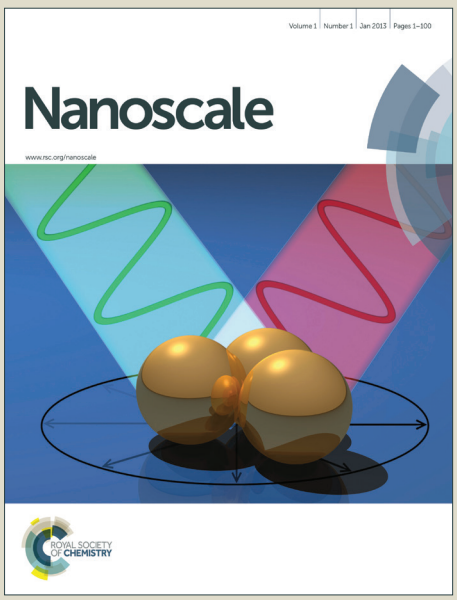

ROYAL SOCIETY OF CHEMISTRY

www.rsc.org/nanoscale

Destruction of Amyloid Fibrils by Graphene through Penetration and Extraction of Peptides

Zaixing Yang[1,‡], Cuicui Ge[1,‡], Jiajia Liu[1], Yu Chong[1], Zonglin Gu[1], Camilo A. Jimenez-Cruz[2], Zhifang Chai[1], and Ruhong Zhou [1,2,3 *]

[1] Institute of Quantitative Biology and Medicine, SRMP and RAD-X, Collaborative Innovation Center of Radiation Medicine of Jiangsu Higher Education Institutions, Soochow University, Suzhou 215123, China

[2] IBM Thomas J. Watson Research Center, Yorktown Heights, NY 10598, USA

[3] Department of Chemistry, Columbia University, New York, NY 10027, USA

‡ These authors contribute equally

*Corresponding author, E-mail: ruhongz@us.ibm.com

Current therapies for Alzheimer's disease (AD) can provide a moderate symptomatic reduction or delay progression at various stages of the disease, but such treatments ultimately do not arrest the advancement of AD. As such, novel approaches for AD treatment and prevention are urgently needed. We here provide both experimental and computational evidence that pristine graphene and graphene-oxide nanosheets can inhibit Aβ peptide monomer fibrillation and disassemble and clear mature amyloid fibrils, thus impacting the central molecular superstructures correlated with AD pathogenesis. Our molecular dynamics simulations for the first time reveal that graphene nanosheets can penetrate and extract a large number of peptides from pre-formed amyloid fibrils; these effects seem to be related to exceptionally strong dispersion interactions between peptides and graphene that are further enhanced by strong π-π stacking between the aromatic residues of extracted Aβ peptides and the graphene surface. Atomic force microscopy images confirm these predictions by demonstrating that mature amyloid fibrils can be cut into pieces

and cleared by graphene oxides. Thioflavin fluorescence assays further illustrate the detailed dynamic processes by which graphene induces inhibition and clearance of monomer aggregation and mature amyloid fibrils, respectively. Cell viability and ROS assays indicate that graphene oxide can indeed mitigate cytotoxicity of Aβ peptide amyloids. Our findings provide new insights into the underlying molecular mechanisms that define graphene-amyloid interaction and suggest that further research on nanotherapies for Alzheimer's and other protein aggregation-related diseases is warranted.

Introduction

The proliferation of Alzheimer's disease (AD) within an aging world population poses a significant challenge to today's health care systems. No immediate cure for AD is in sight - the limited number of small-molecule-based drugs available can help manage AD symptoms, but cannot cure the disease or stop its progression.[1-3] AD is a complex neurodegenerative disorder characterized by cognitive declination involving loss of memory, orientation, judgment, and reasoning.[1-5] Although the molecular mechanisms of AD pathogenesis are not fully understood, extensive evidence indicates that accumulation of abnormally folded amyloid-beta peptides (Aβ) into amyloid aggregates (including oligomers, fibrils, and plaques; particularly oligomers) on neural cell membranes is a critical step in the pathogenesis of the disease.[1-2, 4-5] As such, inhibition of monomer fibrillation and dissociation and clearance of amyloid aggregates are considered the major therapeutic strategies for treating this neurodegenerative disease.[6-7] Recent studies also indicate that fibril plaque formation and neurotoxicity are associated with cell membrane properties in brain tissues, which play a significant role in interactions with peptide oligomers and represent an important alternative target for the development of anti-AD therapies.[8-10] Despite these efforts, the therapeutic application of current anti-AD agents, such as small drug molecules,[6-7] polymers,[11] peptides,[12-13] and metal oxides[14] shows only a moderate inhibitory effect on the monomer fibrillation and a weak capability of dissociating pre-formed amyloid aggregates. It is thus an urgent task to explore and develop more effective therapies for AD.

Nanotechnology and nanoscience, already with wide uses in biomedical areas such as gene delivery,[15] cellular imaging,[16] and tumor therapy,[17] may provide a new direction for the development of anti-AD therapies. In this context, the final goal entails designing effective and biodegradable nanomaterials that inhibit Aβ oligomer formation and clear existing amyloid aggregates. Some early evidence has suggested that particular nanostructures (like specific inorganic nanoparticles and polymeric

nanomaterials) can indeed decrease the probability of Aβ monomers aggregating into fibrils.[18-19] On the other hand, early findings of fibrillation-nanoparticle activity by Dawson and coworkers considered nanoparticles as catalysts for protein fibrillation, in which nanoparticles could significantly enhance the rate of protein fibrillation, or the formation of fibrils.[20] Subsequently, a large number of studies showed the opposite, that nanoparticles could actually inhibit the nucleation step of Aβ fibrillation.[11, 21] There was also evidence that nanoparticles might present a dual role in the Aβ fibrillation, depending on their specific ratios.[22] These studies indicate that it can be a rather complicated situation for nanoparticles' effects on protein fibrillation in general. Meanwhile, few studies have reported that nanomaterials are capable of effectively breaking and clearing pre-formed fibrillar structures,[23] which is a necessary characteristic of AD treatments administered to late-stage patients, in particular. The development of such a capacity would require that a nanomaterial and the Aβ peptide interact more strongly with one another than the peptide does with itself. Interestingly, Zhou and coworkers very recently[24] found that, due to the exceptionally strong dispersion interactions between graphene and lipids, graphene nanosheets can penetrate *E. coli* cell membranes and extract large numbers of phospholipid molecules directly from the lipid bilayer. Inspired by that discovery, we decided to investigate whether graphene nanosheets could also dissociate and clear preformed amyloid aggregates.

Graphene and its derivatives - such as graphene oxide (GO) - are two-dimensional sp^2 carbon nanomaterials that have attracted tremendous attention in biomedical applications due to their unique structural, mechanical and electronic properties.[25-27] The high specific surface area of graphene allows for high-density bio-functionalization in nanotechnology-based drug delivery applications.[26-28] Similarly, its smooth, contiguous topography and biopersistence plays a unique role in foreign-body-induced carcinogenesis and tumor progression.[29-30] Some recent studies have also shown that graphene and graphene-oxide (GO) have strong antibacterial activity,[31-34] which make such materials useful as potential next generation "green" antibiotics. Moreover, because graphene exhibits ultra-high *in vivo* tumor uptake in mice, it is potentially effective for photothermal ablation of tumors.[35] Meanwhile, it

should also be pointed out that upon entering into biological systems, nanoparticles such as graphene nanosheets can rapidly adsorb biomolecules onto their surfaces to form the so-called protein corona to reduce their surface free energy. These protein corona might significantly influence nanoparticles' cellular recognition, uptake, and biological response.[36-38]

Some preliminary work on the interaction between graphene derivatives and amyloid fibrils has been reported. For example, Mahmoudi et al.[39] described a protective role for GO sheets on the amyloid fibrillization process. In this study, the large available surface area of GO sheets was demonstrated to inhibit the process of Aβ fibrillization via adsorption of amyloid monomers. In addition, Mezzenga and coworkers[23] reported that graphene and β-lactoglobulin amyloid fibrils can be combined to create a new class of biodegradable composite materials with adaptable properties. Qu et al. [40] found that thioflavin-modified GO can effectively dissociate amyloid deposits upon near infrared (IR) laser irradiation both in buffer and in mice cerebrospinal fluid. However, the detailed dynamical process and underlying molecular mechanism related to this graphene-induced disassociation and clearance of pre-formed Aβ aggregates has yet to be elucidated; additionally, there is no direct evidence that such dissociation provides neurons any protection against Aβ aggregates.

Here, we show both experimentally and theoretically that graphene nanosheets can inhibit Aβ monomer fibrillization, break and clear pre-formed amyloid fibrils, and also vigorously extract large amounts of peptide directly from fibrils. Our atomic force microscopy (AFM) images show that mature amyloid fibrils are cut into pieces by GO sheets, while fluorescence labeling assays illustrate detailed dynamic processes of aggregate inhibition and dissociation starting from monomer peptides and mature amyloid fibrils, respectively. Molecular dynamics simulations revealed an underlying molecular mechanism: graphene nanosheets can penetrate and extract peptides from the fibrils due to exceptionally strong dispersion interactions between the graphene and peptides. Finally, cell LIVE/DEAD assays were examined to verify the protective effect of GO on nerve cells mediated by breaking and clearing the mature fibrils. To the best of our knowledge, graphene's destructive extraction of peptides from mature

amyloid fibrils, the dynamic details of aggregate inhibition and dissociation, and direct evidence of nerve cell protection have not been previously reported. Furthermore, the molecular mechanism of the disruption of amyloid fibrils by graphene is shown to be somewhat different from that of lipid membranes. [24] In addition to the hydrophobic interaction between nonpolar sidechain of amyloid fibrils and graphene, the strong π–π stacking interaction between the aromatic rings of phenylalanine and graphene also contribute significantly to the destruction of amyloid fibrils. These findings suggest that further work in the *de novo* design of graphene-based nanotherapies for Alzheimer's disease is certainly warranted. Much more study, of course, is needed before graphene can be used in any preclinical therapeutic applications; in particular, more information concerning target peptide specificity is required. One might start by interrogating multiple specific functionalizations of Aβ (such as Aβ coated with binding-partner gangliosides[41]) with which graphene should interact strongly due to its unusually large specific surface area.

Results and Discussion

Molecular dynamics simulations reveal two types of interaction mechanism

In order to investigate the interactions between graphene nanosheets and Aβ amyloid fibrils, various simulation protocols were followed. A pre-formed $A\beta_{16-21}$ (KLVFFA) amyloid fibril containing 24 monomers was simulated in presence of one or two graphene nanosheets with different configurations (see **Fig. S1** and Materials and Methods for more detail). We used this short segment of the Aβ peptide instead of $A\beta_{1-40}$ (used in experiments) as the model system for our molecular dynamics simulations, since (i) it is the characteristic core sequence in Aβ and is also the shortest sequence which is capable of forming amyloid-like fibrils; (ii) it exhibits aggregation kinetics and an X-ray diffraction pattern similar to those seen with the full-length peptide; and (iii) it also exhibits some level of cytotoxicity.[42-44] This choice significantly reduces the extensive computational cost that would be incurred in

simulating longer and more complicated $A\beta_{1-40}$ fibrils.[45] **Figure 1** shows representative trajectories of two graphene nanosheets interacting with the pre-formed Aβ amyloid fibril, first with the two graphene sheets on the same side of the fibril (~3 nm apart; **Fig. 1A**), and then with them on opposite sides of the fibril (**Fig. 1B)**.

Our unbiased simulations clearly show in both cases that the graphene nanosheets are able to disrupt and cut into the pre-formed amyloid fibril within a few hundred nanoseconds; the control runs (without the graphene nanosheets), by contrast, show a stable amyloid fibril structure with all β-sheets intact over the same amount of simulation time. In parallel to graphene interactions with *E. coli* cell membranes,[24] two types of molecular mechanisms, i.e., penetration (insertion) and direct extraction of peptides, were observed in both trajectories. In the former case (**Fig. 1A)**, with the two graphene nanosheets attacking from the same side, the graphene starts to dig into the fibril at around 285 ns. This event is followed by a twisting of the fibril, and a few peptides climb onto the graphene sheet after 425 ns. The phenylalanine residues of extracted Aβ peptides attach to the graphene and form stable π-π stacked interactions.[46] By the 710 ns time point, the two graphene nanosheets have completely cut through the amyloid fibril, leaving the assembly broken into pieces. In the latter case (**Fig. 1B**, and Supplementary **Video S2**), an even stronger disruption to the pre-formed amyloid fibril is observed as the two graphene sheets attack at roughly the same location from both sides. Both graphene sheets start to dig into the fibril around 190 ns, and then the fibril twists significantly at 280 ns. After 520 ns, one sheet successfully cuts into the fibril and the peptides start to climb on both graphene sections. After 870 ns, the fibril has been completely cut into pieces, and many peptides have absorbed onto the graphene sheet involved.

Moreover, two additional sets of simulations were performed to investigate whether graphene can still dissociate amyloid fibrils or not once the constraints on the graphene and peptides are removed. Both the cases with double graphene sheets or single sheet were studied. As shown in Fig. S3A, for the double graphene sheets case, once the constraints were removed, one graphene sheet quickly penetrated into the fibril and cut it into two halves (graphene sheet staying inside the fibril), while the other sheet laid on the fibril surface till the end of the simulation. For the single

graphene case (see Fig. S3B), the graphene also quickly penetrated into the fibril and cut it into two halves, and stayed inside the fibril. It is noteworthy that the peptide extraction was not observed in both simulations. This could be due to the too small graphene size used thus not enough graphene surface available for additional extracted peptides, and/or due to the fact that once laying flat on fibril surface no room available for peptide extraction either. To further illustrate this point, we then doubled the size of the attacking graphene nanosheet in the constrain-free simulations (the length of fibril was also doubled to make sure more than enough peptides are available). As shown in Fig. S4, after the graphene nanosheet (the right one) fully penetrated into the fibril at t = ~50 ns, the peptide extraction process also started. At ~200 ns all the "hanging-out" portion of the inserted graphene was fully covered by the extracted peptides from fibril. This is also consistent with another very recent study where both the inserted bare and serum protein BSA-coated graphene nanosheets can extract lipids from cell membranes to their "hanging-out" portions, but with the BSA-coated one extracting less and covering only those available surfaces aside from BSA[47].

These straightforward observations of insertion/cutting (penetration) support the earlier hypothesis by Mezzenga and coworkers[23] in their proposed sandwich-like structure between a β-lactoglobulin amyloid fibril and graphene, wherein the long β-lactoglobulin amyloid fibril might be cut by graphene oxide sheets. More surprisingly, we found that the graphene nanosheets can vigorously extract single peptide molecules from a mature amyloid fibril onto its own surface.[24] Therefore, both mechanisms (penetration and direct extraction) appear to contribute to the destruction and clearance of pre-formed Aβ amyloid fibrils. Other simulations starting from different initial configurations show similar results (see **Fig. S1** for other trajectories). These predictions from MD simulations are further confirmed by our experiments with AFM imaging and ThT fluorescence assays, as described below.

Graphene "docking" simulations indicate robust peptide extraction

To further verify that this peptide extraction is thermodynamically favorable and not just due to some transient, kinetic effect, we followed a similar procedure to the one reported in our previous study on the graphene/cell-membrane interactions.[24].

We carried out additional simulations with a partially restrained (top-edge restrained) graphene nanosheet "docked" on top of the amyloid fibril (**Fig. 2;** see Materials and Methods for more details). Although this configuration presumably makes direct peptide extraction more difficult, turbulent peptide extractions were, in fact, again observed. During the first 30 ns of the docking simulation, the amyloid fibril moved subtly to adapt to the presence of the graphene (**Fig. 2)**. Once adjusted, peptide molecules close to the sheet started fluctuating, perturbing the once smooth and rigid fibril surface. Strong attraction to the graphene then causes some peptides to climb up the nanosheet surfaces. By t=75 ns, three peptides have been fully abstracted. Notably, this climbing of peptide molecules was observed on both sides of the graphene nanosheet (**Fig. 2**) simultaneously. Again, π-π stacking between the graphene surface and the two phenylalanine residues of the extracted peptide seems to play a dominant role in the successful removal of individual peptides. Hydrophobic interactions between Val/Leu residues of the peptide and the graphene surface also contribute to the interaction, indicating that water dynamics play an important role at the peptide/graphene interface as well.[48-50] More specifically, water play at least two roles in the process: (i) to provide a strong driving force through final drying of hydrophobic residues, particularly phenylalanine, upon binding onto graphene; and (ii) to facilitate as a lubricant for basic residues, such as lysine, to bind to graphene (see Fig. S5 for more details).

It is interesting to note that, since the graphene is uncharged in our simulations, all these turbulent extractions of peptides are driven by comparatively weak and short-ranged dispersion (van der Waals) interactions between the graphene and peptide molecules. Once extracted, both the strong π-π stacking (each contributing up to 10 kcal/mol[46]) and hydrophobic interactions between the graphene and peptides are dominant. This disruption of Aβ peptide fibril structure due to its stronger interaction with graphene than with itself is supported by the experimental results described below.

Fluorescence assays illustrate the dynamic process of GO disruption starting

from both Aβ monomers and mature amyloid fibrils.

To validate the predictions from the above MD simulations, we further investigated the interaction between GO sheets and Aβ peptides with Thioflavin-T (ThT) fluorescence assays and AFM imaging. The morphology of graphene oxides were characterized by AFM. As shown in Fig. S5, the lateral size of small sized graphene oxide (s-GO) is below 15 nm and the lateral size of normal sized GO ranges from 0.5 to 3μm. Here, GO sheets (with lateral size of 500 nm - 3μm) are used instead of pristine graphene in order to ensure high water-dispersability. The dynamic processes of Aβ monomer fibrillation and amyloid fibril dissociation/clearance are examined using $A\beta_{1\text{-}40}$ in the presence and absence of GO. $A\beta_{1\text{-}40}$ was chosen due to its much higher abundance than $A\beta_{1\text{-}42}$ in the human brain, where $A\beta_{1\text{-}42}$ and $A\beta_{1\text{-}40}$ are the main peptide isoforms (hereafter, $A\beta_{1\text{-}40}$ is referred as Aβ peptide in all the experiments unless otherwise explicitly stated). The dynamic processes of aggregation from monomer to fibril, as well as the dissociation from fibril to monomer, can be monitored by a ThT assay, which is a common method for the evaluation of the amyloid fibril formation.

Four different concentrations of GO sheets (0, 12.5, 25, 50 μg/mL) were prepared and added into separate 25 μM Aβ monomer solutions. According to the curves of fluorescence intensity shown in **Fig. 3A**, the fibrillation process of the untreated Aβ (black) followed a conventional nucleated-growth mechanism, which can be described by a lag phase, a rapid exponential growth phase, and a final equilibrium steady state. Once GO nanosheets were introduced to the monomer peptide solutions, the final fluorescence intensity was greatly reduced at all non-zero concentrations tested. The presence of GO sheets at 12.5 μg/mL reduced the fluorescence intensity by more than half, indicating that the GO sheets effectively inhibit the aggregation of monomers and thus slow down the fibrillation process. At higher GO concentrations, such as 25 or 50 μg/mL, the fluorescence intensity was further reduced; in the GO-abundant 50 μg/mL case, the exponential growth of aggregation was also slowed significantly.

Inspired by the strong interactions seen between graphene sheets and the characteristic $A\beta_{16-21}$ (KLVFFA) peptide in the above MD simulations, we further examined the dissociation and clearance effects of GO sheets on pre-formed Aβ fibrils. As shown in **Fig. 3B**, the fluorescence intensity of mature fibrils was strong without GO (shown as little black boxes in **Fig. 3B**) and remained strong with no obvious changes during the entire 12 hour period, indicating that the pre-formed fibrils remained intact in the absence of GO. Once the GO sheets were introduced, a significant reduction in the fluorescence intensity was observed in a manner proportional to the GO concentration. A regression analysis highlights that dissociation dynamics exhibit a rapid exponential-like decay followed by a much slower decline to a quasi-equilibrium state (**Fig. 3B)**. In the case of the 50 μg/mL GO sheets, the fluorescence intensity was reduced by nearly half after 6 hours, indicating that large amounts of Aβ fibrils were dissociated and cleared in this period due to stronger attraction to and disruption from the GO. Overall, these results indicate that GO nanosheets can both effectively inhibit the aggregation of Aβ monomers and dissociate/clear the preformed Aβ amyloid fibrils, as predicted *in silico*.

AFM images show Aβ amyloid fibrils were cut into pieces by GO sheets

To corroborate the above observations, AFM imaging was exploited to directly observe the change in Aβ aggregate morphology upon contact with GO sheets. The untreated Aβ peptides assembled into well-defined fibril structures with lengths of hundreds of nanometers to several micrometers (**Fig. 4A and 4D**). Almost no short fibrils could be observed without GO, indicating that almost full fibrillation occurred under these conditions (25 μM monomers).

After introducing GO nanosheets at 50 μg/mL to the mature peptide fibril assembly and 12 subsequent hours of incubation, we could not observe any clear markers of the fibril presence (**Fig. 4B** and **4E**). Meanwhile, some small and amorphous aggregates were found in the mixed solution, indicating that GO nanosheets were very effective in dissociating and clearing the amyloid fibrils. In

addition to treatment with the above GO sheets (size 0.5-3 μm), ultra-small graphene oxide particles featuring a lateral size of less than 15 nm (denoted as s-GO, and also called graphene quantum dots), were studied in the presence of Aβ amyloids to explore the effect of GO size on disaggregation (**Fig. 4C and 4F**). A similar dissociation of amyloid fibrils was observed in the presence of s-GO; some small residual "plaques" (**Fig. 4C** and **4F)** did, however, persist in solution, indicating that s-GOs are somewhat less effective for fibril clearance than larger GO sheets. This relationship is consistent with our previous findings concerning graphene/cell-membrane interactions, wherein larger graphene sheets demonstrated stronger anti-bacterial capacity.[24] Nonetheless, these results further support the notion that graphene and graphene oxides are able to cut mature amyloid fibrils into pieces for subsequent clearance.

Further analyses of detailed interactions reveal the underlying molecular mechanism

To better understand the penetration and extraction process, we further analyzed the physical interactions between graphene and $A\beta_{16\text{-}21}$ (KLVFFA) peptide fibrils as seen in simulations. **Figure 5** shows interaction potential energy profiles and contact surface areas between the graphene nanosheet and peptide fibrils for both cases shown in **Fig. 1**. The contact surface area is defined as one half of the decrease in the summation of the individual solvent accessible surface area of fibril and graphene with respect to the total solvent accessible surface area of the fibril-graphene complex. Consistent with the above observations, the "binding" energy continuously decreases as strong attraction to the graphene leads to direct extraction of Aβ peptide molecules. The sharp decreases in the binding energy, as seen at times such as ~520 ns in **Fig. 5B** and ~560 ns in **Fig. 5A**, correspond to the peptide extraction events, which are also accompanied by sharp increase in contact surface areas (red curves in **Fig. 5**). Interestingly, on average, when a peptide moves from the fibril onto the graphene surface, it would net gain a ~10 kcal/mol interaction potential energy (see Fig. S6). This strong attraction between graphene and peptides largely comes from

graphene's unique 2D-structure containing all sp^2-carbons, which facilitates exceptionally strong dispersion interactions between graphene and peptide molecules – so strong that self-attraction among peptide molecules within the fibril is overcome. Once extracted, strong π-π stacking and hydrophobic interactions between graphene and the peptides also help to stabilize the dissociated structure. As discussed above, each π-π stack can contribute a substantial 6-10 kcal/mol of binding energy[46] to its parent assembly. This central role for π-π stacking is consistent with observations of the protein HP35 interacting with C_{60} fullerenes, carbon nanotubes, and graphene: graphene interacts most strongly with the protein due to its enhanced π-π stacking with the aromatic residues within the villin headpiece sequence.[51] Meanwhile, the strong hydrophobic interactions between Aβ peptide residues Val, Leu, Phe, and graphene resembles hydrophobic packing in many biomolecular self-assemblies. In systems involving cell membrane formation and protein folding, many recent studies[48-50] have shown that nanoscale dehydration can provide a significant driving force for the assembly of stable complexes.

The potential of mean force (PMF) was further calculated to compare the strength of binding for the peptide with fibril or with graphene. Three sets of umbrella sampling simulations were performed to estimate the PMF for the peptide in the interior of fibril, at the terminal of fibril, and peptide-graphene complex. Fig. S7 shows the sketches of three binding systems, with the PMF reaction coordinate of the peptide in the interior and at the terminal of fibril systems set to be vertical and along the fibril axis (see arrows in Fig. S7A and B), respectively, while the peptide-graphene system set to be along the norm of graphene (Fig. S7C). The PMF curves were obtained by using 25, 31 and 43 sampling windows along the reaction coordinates of the peptide in the interior, at the terminal of fibril, and the peptide-graphene complex, respectively. The binding free energy for peptide in the interior and at the terminal of fibril is calculated to be approximately -16.34 and -8.24 kcal/mol (Fig. S7A and B), while it is -19.46 kcal/mol for peptide with graphene, which is about 3.12 and 11.4 kcal/mol more favorable than the peptide in

the interior or at the terminal of fibril (Fig. S7A and B). These results further confirm that extraction of peptides from fibril to the graphene surface is energetically favorable.

LIVE/DEAD and ROS assays reveal that GO can mitigate cytotoxicity of A$\beta_{1\text{-}40}$

Fluorescence-based LIVE/DEAD assays were employed to evaluate the cytotoxic effects of A$\beta_{1\text{-}40}$ on PC12 cells upon GO treatment. Images of live and dead cells after treatment (and incubation for 48 h) are provided in **Fig.6**. As compared to the control, no dead cells were observed in the purely GO-treated groups (2rd column in **Fig. 6**), indicating that GO causes no noticeable toxicity to PC12 cells. This observation is in contrast with marked graphene cytotoxicity seen in bacterial cells such as *E. coli*, which express none of the protective serum proteins typical in mammalian cells[24]. In the purely A$\beta_{1\text{-}40}$-treated group, a significant quantity of dead cells was observed (3rd column in **Fig. 6**), as highlighted by the bright red fluorescence spots seen in the associated images. Once GO was added into the A$\beta_{1\text{-}40}$-treated group (pre-incubated with A$\beta_{1\text{-}40}$ for 2 h), only very small quantity of dead cells was observed (4th column in **Fig. 6**). Notably, the β-amyloid itself is a source of free radicals.[52] One possible mechanism for initiating apoptosis in the cells studied could involve peptide-generated free radicals that lead to lipid peroxidation and oxidative stress. Therefore, an intracellular reactive oxygen species (ROS) assay was also conducted. As shown in the second row of **Fig. 6**, A$\beta_{1\text{-}40}$ stimulated significant formation of ROS, indicating that generation of ROS could constitute a possible pathway for A$\beta_{1\text{-}40}$-mediated cytotoxicity in neurons. After introducing GO, the formation of ROS was substantially reduced in a manner consistent with the live/dead assay. These findings indicate that the cytotoxic effects of A$\beta_{1\text{-}40}$ on PC12 cells can be significantly mitigated by GO sheets, suggesting that GO sheets are capable of effectively clearing toxic A$\beta_{1\text{-}40}$ peptides in cells.

Finally, it should be noted that while pristine graphene was used in our

simulations, the poor solubility of graphene dictated that GO be used in the experiments. However, in our previous study of graphene interactions with bacterial cell-membranes,[24] we did simulate GO nanosheets using the Lerf-Klinowski model ($C_{10}O_1(OH)_1(COOH)_{0.5}$), which provides representative outcomes from standard oxidation processes.[53-55] The simulation results related to GO nanosheets were largely consistent with those from pristine graphene: GO demonstrated only slightly abrogated intensity in its interaction with cell membranes.[24] It is also relevant to point out that recent experiments have shown that large unoxidized residual graphene-like regions can exist on GO nanosheets (so-called "sp^2-domains"),[53, 56-57] with up to ~60% of the surface remaining undisturbed.[56] These large unoxidized sp^2-domains resemble pristine graphene nanosheets that exhibit efficacy in clearing Aβ peptide aggregates in simulations.

Conclusion

In this paper, the graphene-induced clearance of mature Aβ amyloid fibrils has been investigated using both experimental and theoretical approaches. Severe insertion/cutting (penetration) and destructive extraction of Aβ peptide molecules were identified as two molecular mechanisms responsible for this clearance. To the best of our knowledge, this surprising direct extraction of peptide molecules from fibrils has not been reported previously in literature; the effect is reminiscent of the turbulent, graphene-mediated abstraction of phospholipid molecules from bacterial cell-membranes.[24] The strong attraction between graphene and amyloid fibrils seems to be largely derived from graphene's unique 2D-structure containing all sp^2-carbons, which facilitates exceptionally strong dispersion interactions between graphene and peptide molecules. Once extracted, this attraction is further enhanced by strong π-π stacking between Aβ peptide aromatic residues and the graphene surface. The destructive peptide extraction mediated by graphene nanosheets is also found to be robust even with the graphene "standing still" in space (i.e., docked). These

predictions derived from simulations were supported by both AFM images and ThT fluorescence assays, which illustrated the capability of graphene oxide sheets in inhibiting Aβ monomer fibrillation and clearing mature fibrils. Cell viability assays also revealed that graphene oxide could indeed mitigate cytotoxicity of Aβ peptide amyloids.

The severity of observed graphene insertion and destructive peptide extraction suggests that graphene nanosheets can effectively inhibit Aβ monomer fibrillization and clear the pre-formed amyloid fibrils (or other types of aggregates) that form the major pathological elements of AD. Similar mechanisms of amyloid and aggregate destruction may also be relevant to removing toxic structures implicated in other protein conformational diseases (PCD), as well. Naturally, more studies are needed before any graphene-based therapies can be applied in clinical settings; work elucidating target specificity, and drug delivery, in particular on how to cross the blood-brain barrier (BBB) is required (perhaps mediated through multiple specific functionalizations of graphene).[58] Future work should also involve more *in vivo, in vitro* and *in silico* studies to improve the efficacy of these graphene-based nanotherapies. More importantly, the biocompatibility (and potential nanotoxicity) of these designed nanomaterials remains an issue to be addressed before their wide application to human therapies. Nonetheless, we hope the current work sets some foundation for understanding the underlying molecular mechanisms that describe graphene-amyloid interactions and provides further leads in the development of nanotherapies for Alzheimer's and other protein conformational diseases.

Materials and Methods

Materials. Graphene oxide (dimension from 0.5 μm to 3 μm) was purchased from Chengdu Organic Chemical Company, Chinese Academy of Science. Small graphene oxide quantum dots (s-GO, size < 15 nm) were purchased from Nanjing XFNano Material Tech Co., Ltd. The purchased graphene oxides are further

characterized by AFM (images shown in Fig. S8). It is clear that the lateral size of small-sized graphene oxide (s-GO) is indeed below 15 nm, and the lateral size of normal-sized GO ranges from 0.5 to 3μm. Highly purified (purity > 97%) A$\beta_{1\text{-}40}$ was obtained from Hangzhou Chinese Peptide Company. Thioflavin T, 1,1,1,3,3,3-hexafluoro-2-propanol (HFIP), and dimethyl sulfoxide (DMSO) were bought from Sigma-Aldrich. CCK-8 assay kits were obtained from Dojindo Laboratories.

Preparation of monomeric peptide and fibrillar samples. Lyophilized A$\beta_{1\text{-}40}$ was stored in sealed glass vials at -80°C. Prior to use, each vial of peptide was dissolved in the 100% HFIP to a concentration of 1 mM. The HFIP was then allowed to evaporate in the fume hood until the solution became clear. The resulting peptide films were dried under vacuum and dissolved in DMSO to a final concentration of 1 mM to serve as a stock solution of monomeric peptide. For the fibrillation, the stock solution was added to phosphate-buffered saline (PBS buffer, pH 7.4) to yield a 50 μM A$\beta_{1\text{-}40}$ solution, immediately vortexed for 30 s, and stirred at 37℃ for 24 h.

ThT fluorescence assay. To investigate the influence of GO on A$\beta_{1\text{-}40}$ monomers and fibrils, different amounts of nanoparticle were added to 25 μM A$\beta_{1\text{-}40}$ solution (either of stock solution or containing mature fibrils). The final concentration of GO was adjusted to 12.5, 25, 50 μg/mL. The resultant mixtures were stirred at room temperature and the fibrillation process of A$\beta_{1\text{-}40}$ was monitored by a ThT assay every half hour after adding the mixture of A$\beta_{1\text{-}40}$ and GO into 20 μm ThT solution. Photoluminescence spectra of the ThT assay were recorded on a Synergy NEO HTS multi-mode microplate reader (Biotek, USA) with an excitation wavelength of 450 nm and an emission wavelength of 485 nm.

Atomic Force Microscopy. To further verify the effects of GO on A$\beta_{1\text{-}40}$ fibrils, two sizes of GO (l-GO:0.5-3 μm; s-GO: <15 nm; both at a concentration of 50 μg/mL) were individually mixed with 25 μM A$\beta_{1\text{-}40}$ fibrils and stirred at room temperature for 12 h. Each sample was then deposited on the surface of fresh mica, and analysis was performed using an AFM (Nanoscope Icon, Veeco, USA) in tapping mode.

Cell LIVE/DEAD and ROS assay. PC-12 cells were plated on 24-well plates for 24 h, and then the DMEM medium was respectively replaced by a dispersion of GO, $A\beta_{1\text{-}40}$, and a mixture of GO/$A\beta_{1\text{-}40}$ (in which GO was introduced after incubation with $A\beta_{1\text{-}40}$ for 2 h). After 48 h of incubation, cells were treated with a Live/Dead viability assay and analyzed by a fluorescence microscope (Olympus, Japan). The viable cells fluoresce at green wavelengths, whereas nuclei of dead cells emit red light.

2,7-Dichlorodihydrofluorescein diacetate (DCFH-DA, Sigma) is not fluorescent until it is oxidized by the intracellular ROS. Measurements of the generation of ROS were conducted by incubating 15×10^4 cells /per well in the 6-well plate for 24 h. The DMEM medium was respectively replaced by a dispersion of GO, $A\beta_{1\text{-}40}$, and a mixture of GO/$A\beta_{1\text{-}40}$ (in which GO was introduced after incubation with $A\beta_{1\text{-}40}$ for 2 h). After 48 h of incubation, cells were stained with DCFH-DA for 30 min at 37 °C. Cells were then washed 3 times with PBS buffer and analyzed using a fluorescence microscope (Olympus, Japan) at an excitation wavelength of 488 nm and emission wavelengths of 530 and 610 nm for DCFH-DA.

Computer Simulation Methods. We carried out molecular dynamics simulations of graphene nanosheets interacting with a KLVFFA β-sheet in four different models, each differing in the number of graphene nanosheets and their location with respect to the β-sheet. For the systems containing two graphene nanosheets, two possible configurations were studied: one with both nanosheets placed parallel to each other on the same side of the β-sheet and perpendicular to its main axis (see **Fig. 1A**), and the other with each nanosheet placed on the opposite sides of the β-sheet and also perpendicular to its main axis (see **Fig. 1B**). Similarly, two different configurations of systems with a single graphene nanosheet were simulated. In one case, the graphene nanosheet was hung over the top of the β-sheet (see **Fig. 2A**), whereas in the other case, the graphene nanosheet was placed perpendicular to the main axis of the β-sheet (see **Fig. S1**).

In this study, the raw KLVFFA β-sheet configuration was constructed using the

X-ray crystal structure from Eisenberg and coworkers[43] deposited in the Protein Data Bank (PDB code: 3OW9) as a template. This crystal structure consists of two stable, flat, antiparallel β-sheets, each containing six anti-parallel peptides. This β-sheet was then extended along its long-axis to twice its original length, resulting in a longer anti-parallel (12×2)-β-sheet, which became the model for Aβ amyloid fibrils in our simulations.

The coordinates of graphene nanosheets were generated using the nanotube builder plugin of VMD software.[59] The sizes of the graphene nanosheets are 1.99× 4.92 nm^2, 3.26×4.92 nm^2, 1.99×4.92 nm^2, and 1.57×4.92 nm^2 for each of the four systems described above, respectively. The combined systems of nanosheets and model Aβ amyloid fibrils were solvated in water boxes with a minimum distance between solute and the edges of the box of at least 1.2 nm. The initial minimum distance between any heavy atoms of the β-sheet and the graphene nanosheet was at least 0.5 nm. Finally, 24 Cl^- ions were added into solution to neutralize each system. The resultant simulation boxes contained 69,236, 80,000, 34,828, and 62,005 atoms for the four respective systems. The simple point charge (SPC) model [60] was used for all water molecules, while the OPLS-AA force field[61] was used for the KLVFFA peptide. The carbon atoms of graphene were modeled as uncharged Lennard-Jones particles with a cross-section of σ_{cc}= 0.34 nm and potential well depth of ε_{cc} = 0.3598 kJ mol^{-1}. Carbon-carbon bond lengths and bond angles were maintained by harmonic potentials with spring constants of 392,460 kJ $mol^{-1}nm^{-2}$ and 527 kJ $mol^{-1}rad^{-2}$ respectively.

MD simulations were performed using the Gromacs-4.6.3 package,[62] and VMD[59] was used for trajectory visualization and analysis. Constant temperature (at 310 K) and pressure (at 1 atm) were maintained by using a v-rescale thermostat[63] and Parrinello-Rahmann pressure coupling scheme,[64] respectively. Periodic boundary conditions were applied in all directions. The particle-mesh Ewald method with a real space cutoff of 1.2 nm was used to treat long-range electrostatic interactions,[65] whereas vdW interactions were treated with a cutoff distance of 1.2 nm. LINCS[66]

was applied to constrain bond lengths within the solute and the SETTLE[67] algorithm was used to constrain water bond lengths and angles. Position restraints were applied to the graphene nanosheet and the peptides for 100 ps to allow for solute equilibration before production runs. For all production simulations, the positions of sixteen carbon atoms in four carbon rings at one of the corners were constrained by using a positional restraint (see Fig. S9A, B and D for more details), while the other carbon atoms were left free to move. The C_α carbons of the terminal four peptide chains in the β-sheet were also restrained, while the remaining peptides were allowed to move freely (Fig. S9). For the graphene "docking" simulations, the entire top row of 6-membered rings was restrained (Fig. S9C). A time step of 2.0 fs was used in all production simulations, and coordinates were collected every 10 ps. For each system, five independent runs were performed for improved statistics. The simulation length for each run was about 1 μs; the total aggregate simulation time for this study was > 20.0 μs. The setup of umbrella samplings are shown in Supporting Information.

ACKNOWLEDGMENTS

We thank Bruce Berne, Yuliang Zhao, Seung-gu Kang, Chunying Chen, Andre Nel, Bo Zhou, Shengtang Liu, Baoyu Li and Weifeng Li for helpful discussions. This work was partially supported by the National Natural Science Foundation of China under Grant Nos. 11374221, 11574224, 11404233, 21320102003, 21207164 the National Basic Research Program of China (2014CB931900). A Project Funded by the Priority Academic Program Development of Jiangsu Higher Education Institutions (PAPD), and Jiangsu Provincial Key Laboratory of Radiation Medicine and Protection. RZ acknowledges the support from IBM Blue Gene Science Program.

.

Author contributions

R.H.Z. conceived and designed the simulations and experiments. Z.X.Y., J.J.L., Z.L.G. performed the simulations. C.C.G, Y.C. performed the experiments. R.H.Z., Z.X.Y., C.C.G., Y.C., Z.L.G. and C.J. analyzed the data. R.H.Z., C.C.G. and Z.X.Y. co-wrote the paper. All authors discussed the results and commented on the manuscript.

Additional information

The authors declare no competing financial interests. Electronic supplementary information (ESI) are available: other representative trajectories for all the four types of simulated models with double or single graphene nanosheets; instruction to the video; two representative trajectories to show graphene sheet(s) spontaneously penetrating into the fibril; role of interfacial water in assisting graphene's insertion into fibril; AFM images of s-GO and GO; potential of mean force; sketches of restraints in all four types of simulated systems. Correspondence and requests for materials should be addressed to R.H.Z.

Reference

1. Harper, J. D.; Lansbury, P. T., Models of amyloid seeding in alzheimier's disease and scrapie: Mechanistic truths and physiological consequences of the time-dependent solubility of amyloid proteins. *Annu. Rev. Biochem.* **1997,** *66*, 385-407.

2. Gregersen, N.; Bross, P.; Vang, S.; Christensen, J. H., Protein misfolding and human disease. *Annu. Rev. Genomics Hum. Genet.* **2006,** *7*, 103-124.

3. Holtzman, D. M.; Morris, J. C.; Goate, A. M., Alzheimer's disease: The challenge of the second century. *Sci. Transl. Med.* **2011,** *3* (77), 17.

4. Dobson, C. M., Protein folding and misfolding. *Nature* **2003,** *426* (6968), 884-890.

5. Lee, J.; Culyba, E. K.; Powers, E. T.; Kelly, J. W., Amyloid-beta forms fibrils by nucleated conformational conversion of oligomers. *Nat. Chem. Biol.* **2011,** *7* (9), 602-9.

6. Morshedi, D.; Rezaei-Ghaleh, N.; Ebrahim-Habibi, A.; Ahmadian, S.; Nemat-Gorgani, M., Inhibition of amyloid fibrillation of lysozyme by indole derivatives - possible mechanism of action. *Febs J* **2007,** *274* (24), 6415-6425.

7. Howlett, D.; Cutler, P.; Heales, S.; Camilleri, P., Hemin and related porphyrins inhibit beta-amyloid aggregation. *FEBS Lett.* **1997,** *417* (2), 249-251.

8. Drolle, E.; Hane, F.; Lee, B.; Leonenko, Z., Atomic force microscopy to study molecular

mechanisms of amyloid fibril formation and toxicity in alzheimer's disease. *Drug. Metab. Rev.* **2014,** *46* (2), 207-223.

9. Jang, H.; Arce, F. T.; Ramachandran, S.; Capone, R.; Lal, R., et al., Beta-barrel topology of alzheimer's beta-amyloid ion channels. *J. Mol. Biol.* **2010,** *404* (5), 917-934.

10. Burke, K. A.; Yates, E. A.; Legleiter, J., Biophysical insights into how surfaces, including lipid membranes, modulate protein aggregation related to neurodegeneration. *Front. Neurol.* **2013,** *4*, 17-17.

11. Cabaleiro-Lago, C.; Quinlan-Pluck, F.; Lynch, I.; Lindman, S.; Minogue, A. M., et al., Inhibition of amyloid-β protein fibrillation by polymeric nanoparticles. *J. Am. Chem. Soc.* **2008,** *130* (46), 15437-15443.

12. Frydman-Marom, A.; Rechter, M.; Shefler, I.; Bram, Y.; Shalev, D. E., et al., Cognitive-performance recovery of alzheimer's disease model mice by modulation of early soluble amyloidal assemblies. *Angew. Chem. Int. Edit.* **2009,** *48* (11), 1981-1986.

13. Bronfman, F. C.; Garrido, J.; Alvarez, A.; Morgan, C.; Inestrosa, N. C., Laminin inhibits amyloid-β-peptide fibrillation. *Neurosci. Lett.* **1996,** *218* (3), 201-203.

14. Barnham, K. J.; Kenche, V. B.; Ciccotosto, G. D.; Smith, D. P.; Tew, D. J., et al., Platinum-based inhibitors of amyloid-β as therapeutic agents for alzheimer's disease. *Proc. Natl. Acad. Sci. U. S. A.* **2008,** *105* (19), 6813-6818.

15. Rosi, N. L.; Giljohann, D. A.; Thaxton, C. S.; Lytton-Jean, A. K. R.; Han, M. S., et al., Oligonucleotide-modified gold nanoparticles for intracellular gene regulation. *Science* **2006,** *312* (5776), 1027-1030.

16. Michalet, X.; Pinaud, F. F.; Bentolila, L. A.; Tsay, J. M.; Doose, S., et al., Quantum dots for live cells, in vivo imaging, and diagnostics. *Science* **2005,** *307* (5709), 538-544.

17. Grossman, J. H.; McNeil, S. E., Nanotechnology in cancer medicine. *Phys. Today* **2012,** *65* (8), 38-42.

18. Yoo, S. I.; Yang, M.; Brender, J. R.; Subramanian, V.; Sun, K., et al., Inhibition of amyloid peptide fibrillation by inorganic nanoparticles: Functional similarities with proteins. *Angew. Chem. Int. Edit.* **2011,** *50* (22), 5110-5115.

19. Xiao, L.; Zhao, D.; Chan, W.-H.; Choi, M. M. F.; Li, H.-W., Inhibition of beta 1-40 amyloid fibrillation with n-acetyl-l-cysteine capped quantum dots. *Biomaterials* **2010,** *31* (1), 91-98.

20. Colvin, V. L.; Kulinowski, K. M., Nanoparticles as catalysts for protein fibrillation. *Proc. Natl. Acad. Sci. U. S. A.* **2007,** *104* (21), 8679-8680.

21. Cabaleiro-Lago, C.; Lynch, I.; Dawson, K. A.; Linse, S., Inhibition of iapp and iapp((20-29)) fibrillation by polymeric nanoparticles. *Langmuir* **2010,** *26* (5), 3453-3461.

22. Cabaleiro-Lago, C.; Quinlan-Pluck, F.; Lynch, I.; Dawson, K. A.; Linse, S., Dual effect of amino modified polystyrene nanoparticles on amyloid beta protein fibrillation. *Acs. Chem. Neurosci.* **2010,** *1* (4), 279-287.

23. Li, C.; Adamcik, J.; Mezzenga, R., Biodegradable nanocomposites of amyloid fibrils and graphene with shape-memory and enzyme-sensing properties. *Nat Nanotechnol* **2012,** *7* (7), 421-427.

24. Tu, Y.; Lv, M.; Xiu, P.; Huynh, T.; Zhang, M., et al., Destructive extraction of phospholipids from escherichia coli membranes by graphene nanosheets. *Nat Nanotechnol* **2013,** *8* (8), 594-601.

25. Geim, A. K., Graphene: Status and prospects. *Science* **2009,** *324* (5934), 1530-1534.

26. Feng, L.; Liu, Z., Graphene in biomedicine: Opportunities and challenges. *Nanomedicine* **2011,** *6* (2), 317-324.

27. Sanchez, V. C.; Jachak, A.; Hurt, R. H.; Kane, A. B., Biological interactions of graphene-family nanomaterials: An interdisciplinary review. *Chem. Res. Toxicol.* **2011,** *25* (1), 15-34.

28. Liu, Z.; Robinson, J. T.; Sun, X.; Dai, H., Pegylated nanographene oxide for delivery of water-insoluble cancer drugs. *J. Am. Chem. Soc.* **2008,** *130* (33), 10876-10877.

29. Okada, F., Beyond foreign-body-induced carcinogenesis: Impact of reactive oxygen species derived from inflammatory cells in tumorigenic conversion and tumor progression. *Int. J. Cancer* **2007,** *121* (11), 2364-2372.

30. Soldano, C.; Mahmood, A.; Dujardin, E., Production, properties and potential of graphene. *Carbon* **2010,** *48* (8), 2127-2150.

31. Hu, W.; Peng, C.; Luo, W.; Lv, M.; Li, X., et al., Graphene-based antibacterial paper. *ACS Nano* **2010,** *4* (7), 4317-4323.

32. Akhavan, O.; Ghaderi, E., Toxicity of graphene and graphene oxide nanowalls against bacteria. *ACS Nano* **2010,** *4* (10), 5731-5736.

33. Liu, S.; Zeng, T. H.; Hofmann, M.; Burcombe, E.; Wei, J., et al., Antibacterial activity of graphite, graphite oxide, graphene oxide, and reduced graphene oxide: Membrane and oxidative stress. *ACS Nano* **2011,** *5* (9), 6971-6980.

34. Krishnamoorthy, K.; Veerapandian, M.; Zhang, L.-H.; Yun, K.; Kim, S. J., Antibacterial efficiency of graphene nanosheets against pathogenic bacteria via lipid peroxidation. *J. Phys. Chem. C* **2012,** *116* (32), 17280-17287.

35. Yang, K.; Zhang, S.; Zhang, G.; Sun, X.; Lee, S.-T., et al., Graphene in mice: Ultrahigh in vivo tumor uptake and efficient photothermal therapy. *Nano Lett.* **2010,** *10* (9), 3318-3323.

36. Monopoli, M. P.; Aberg, C.; Salvati, A.; Dawson, K. A., Biomolecular coronas provide the biological identity of nanosized materials. *Nat. Nanotechnol.* **2012,** *7* (12), 779-786.

37. Mahmoudi, M.; Monopoli, M. P.; Rezaei, M.; Lynch, I.; Bertoli, F., et al., The protein corona mediates the impact of nanomaterials and slows amyloid beta fibrillation. *Chembiochem* **2013,** *14* (5), 568-572.

38. Ge, C.; Tian, J.; Zhao, Y.; Chen, C.; Zhou, R., et al., Towards understanding of nanoparticle-protein corona. *Arch. Toxicol.* **2015,** *89* (4), 519-539.

39. Mahmoudi, M.; Akhavan, O.; Ghavami, M.; Rezaee, F.; Ghiasi, S. M. A., Graphene oxide strongly inhibits amyloid beta fibrillation. *Nanoscale* **2012,** *4* (23), 7322-7325.

40. Li, M.; Yang, X.; Ren, J.; Qu, K.; Qu, X., Using graphene oxide high near-infrared absorbance for photothermal treatment of alzheimer's disease. *Adv. Mater.* **2012,** *24* (13), 1722-1728.

41. Choo-Smith, L. P.; Garzon-Rodriguez, W.; Glabe, C. G.; Surewicz, W. K., Acceleration of amyloid fibril formation by specific binding of abeta-(1-40) peptide to ganglioside-containing membrane vesicles. *J. Biol. Chem.* **1997,** *272* (37), 22987-90.

42. Xue, W. F.; Hellewell, A. L.; Gosal, W. S.; Homans, S. W.; Hewitt, E. W., et al., Fibril fragmentation enhances amyloid cytotoxicity. *J. Biol. Chem.* **2009,** *284* (49), 34272-34282.

43. Colletier, J. P.; Laganowsky, A.; Landau, M.; Zhao, M. L.; Soriaga, A. B., et al., Molecular basis for amyloid-β polymorphism. *Proc. Natl. Acad. Sci. U. S. A.* **2011,** *108* (41), 16938-16943.

44. Luhrs, T.; Ritter, C.; Adrian, M.; Riek-Loher, D.; Bohrmann, B., et al., 3d structure of alzheimer's amyloid-β_{1-42} fibrils. *Proc. Natl. Acad. Sci. U. S. A.* **2005,** *102* (48), 17342-17347.

45. Lu, J. X.; Qiang, W.; Yau, W. M.; Schwieters, C. D.; Meredith, S. C., et al., Molecular structure of beta-amyloid fibrils in alzheimer's disease brain tissue. *Cell* **2013,** *154* (6), 1257-68.

46. Yang, Z.; Wang, Z.; Tian, X.; Xiu, P.; Zhou, R., Amino acid analogues bind to carbon nanotube via

pi-pi interactions: Comparison of molecular mechanical and quantum mechanical calculations. *J. Chem. Phys.* **2012,** *136* (2), 025103.

47. Duan, G.; Kang, S. G.; Tian, X.; Garate, J. A.; Zhao, L., et al., Protein corona mitigates the cytotoxicity of graphene oxide by reducing its physical interaction with cell membrane. *Nanoscale* **2015**.

48. Liu, P.; Huang, X.; Zhou, R.; Berne, B. J., Observation of a dewetting transition in the collapse of the melittin tetramer. *Nature* **2005,** *437* (7055), 159-62.

49. Zhou, R.; Huang, X.; Margulis, C. J.; Berne, B. J., Hydrophobic collapse in multidomain protein folding. *Science* **2004,** *305* (5690), 1605-9.

50. Berne, B. J.; Weeks, J. D.; Zhou, R., Dewetting and hydrophobic interaction in physical and biological systems. *Annu. Rev. Phys. Chem.* **2009,** *60*, 85-103.

51. Zuo, G.; Zhou, X.; Huang, Q.; Fang, H.; Zhou, R., Adsorption of villin headpiece onto graphene, carbon nanotube, and c60: Effect of contacting surface curvatures on binding affinity. *J. Phys. Chem. C* **2011,** *115*, 23323-23328.

52. Hensley, K.; Carney, J. M.; Mattson, M. P.; Aksenova, M.; Harris, M., et al., A model for beta-amyloid aggregation and neurotoxicity based on free-radical generation by the peptide - relevance to alzheimer-disease. *Proc. Natl. Acad. Sci. U. S. A.* **1994,** *91* (8), 3270-3274.

53. Lerf, A.; He, H.; Forster, M.; Klinowski, J., Structure of graphite oxide revisited ‖ . *J. Phys. Chem. B* **1998,** *102* (23), 4477-4482.

54. Shih, C. J.; Lin, S.; Sharma, R.; Strano, M. S.; Blankschtein, D., Understanding the ph-dependent behavior of graphene oxide aqueous solutions: A comparative experimental and molecular dynamics simulation study. *Langmuir* **2012,** *28* (1), 235-41.

55. Medhekar, N. V.; Ramasubramaniam, A.; Ruoff, R. S.; Shenoy, V. B., Hydrogen bond networks in graphene oxide composite paper: Structure and mechanical properties. *ACS Nano* **2010,** *4* (4), 2300-2306.

56. Gómez-Navarro, C.; Meyer, J. C.; Sundaram, R. S.; Chuvilin, A.; Kurasch, S., et al., Atomic structure of reduced graphene oxide. *Nano Lett.* **2010,** *10* (4), 1144-1148.

57. Ganguly, A.; Sharma, S.; Papakonstantinou, P.; Hamilton, J., Probing the thermal deoxygenation of graphene oxide using high-resolution in situ x-ray-based spectroscopies. *J. Phys. Chem. C* **2011,** *115* (34), 17009-17019.

58. Bramini, M.; Ye, D.; Hallerbach, A.; Raghnaill, M. N.; Salvati, A., et al., Imaging approach to mechanistic study of nanoparticle interactions with the blood-brain barrier. *ACS Nano* **2014,** *8* (5), 4304-4312.

59. Humphrey, W.; Dalke, A.; Schulten, K., Vmd: Visual molecular dynamics. *J. Mol. Graph.* **1996,** *14* (1), 33-&.

60. Choudhury, N.; Pettitt, B. M., On the mechanism of hydrophobic association of nanoscopic solutes. *J. Am. Chem. Soc.* **2005,** *127* (10), 3556-3567.

61. Jorgensen, W. L.; Maxwell, D. S.; Tirado-Rives, J., Development and testing of the opls all-atom force field on conformational energetics and properties of organic liquids. *J. Am. Chem. Soc.* **1996,** *118* (45), 11225-11236.

62. Lindahl, E.; Hess, B.; van der Spoel, D., Gromacs 3.0: A package for molecular simulation and trajectory analysis. *J. Mol. Model.* **2001,** *7* (8), 306-317.

63. Bussi, G.; Donadio, D.; Parrinello, M., Canonical sampling through velocity rescaling. *J. Chem. Phys.* **2007,** *126* (1), 7.

64. Parrinello, M.; Rahman, A., Polymorphic transitions in single-crystals - a new molecular-dynamics method. *J. Appl. Phys.* **1981,** *52* (12), 7182-7190.

65. Selkoe, D. J., Alzheimer's disease: Genes, proteins, and therapy. *Physiol. Rev.* **2001,** *81* (2), 741-766.

66. Hess, B.; Bekker, H.; Berendsen, H. J. C.; Fraaije, J., Lincs: A linear constraint solver for molecular simulations. *J. Comput. Chem.* **1997,** *18* (12), 1463-1472.

67. Miyamoto, S.; Kollman, P. A., Settle - an analytical version of the shake and rattle algorithm for rigid water models. *J. Comput. Chem.* **1992,** *13* (8), 952-962.

Figure Captions

Figure 1. **Graphene nanosheet Penetration and Aβ peptide extraction**. Two representative trajectories of graphene nanosheet insertion and peptide extraction, featuring (A) two graphene sheets attacking a pre-formed Aβ amyloid fibril from the same side, and (B) the two graphene sheets attacking from both sides. The Aβ peptides (consisting of a total of 24 monomers) are shown in a cartoon representation, with the two aromatic phenylalanine residues shown in dark blue sticks. The graphene sheet is shown as an orange sheet. Extracted peptides are highlighted with their phenylalanine residues depicted in larger van der Waals spheres.

Figure 2. Aβ peptide extraction by graphene in docking simulations. A representative trajectory of a "top-edge-restrained" graphene nanosheet docked at the edge of the Aβ amyloid fibril. The simulation time is indicated in each snapshot, with the last snapshot shown from more angles (rotated counterclockwise by the indicated angle from each preceding frame to obtain the current view). Color settings are the same as in **Fig. 1**.

Figure 3. Kinetics of monomer fibrillation and fibril dissociation with or without GO. The dynamic processes of A$\beta_{1\text{-}40}$ monomer fibrillation (A) and A$\beta_{1\text{-}40}$ amyloid fibril dissociation (B) in the presence and absence of GO at different concentrations. The results indicate that GO nanosheets can not only effectively inhibit the aggregation of Aβ monomers, but also dissociate and clear pre-formed Aβ amyloid fibrils.

Figure 4. AFM images of Aβ fibrils with or without GO with different dimensions. AFM images of 25 μM amyloid fibrils mixed with water (A, D), or large GO sheets with a lateral size of 0.5 - 3 μm (B, E) and small GO nanosheets with a lateral size of less than 15 nm (s-GO; C,F) on substrate mica for 12 h. The images A, B, C show one typical view, while D, E, F show the same image but at higher magnification.

Figure 5. Interaction energy profiles. Time evolution of the interaction potential energy between the graphene nanosheet and the peptide amyloid fibril (in black), alongside the contact area between the graphene and peptides (in red) for the representative trajectories shown in **Fig. 1** (A, for the two graphene sheets on the same side, and B, for the graphene sheets on both sides). The sharp decreases in the interaction energies correlate well with the significant increases in the contact surface area.

Figure 6. Effects of GO on the cytotoxicity of A$\beta_{1\text{-}40}$. The top images show the live

and dead stains for PC-12 cells after treatment with GO or Aβ for 48 h. In the $A\beta_{1\text{-}40}$+GO case, the GO was introduced after incubation with $A\beta_{1\text{-}40}$ for 2 h. The viable cells fluoresce in green, whereas nuclei of dead cells emit red light. The bottom images show the ROS assay for PC-12 cells after treatment for 48 h. Control: untreated cells, [$A\beta_{1\text{-}40}$] = 50 μM, [GO] = 12.5 μg/mL.

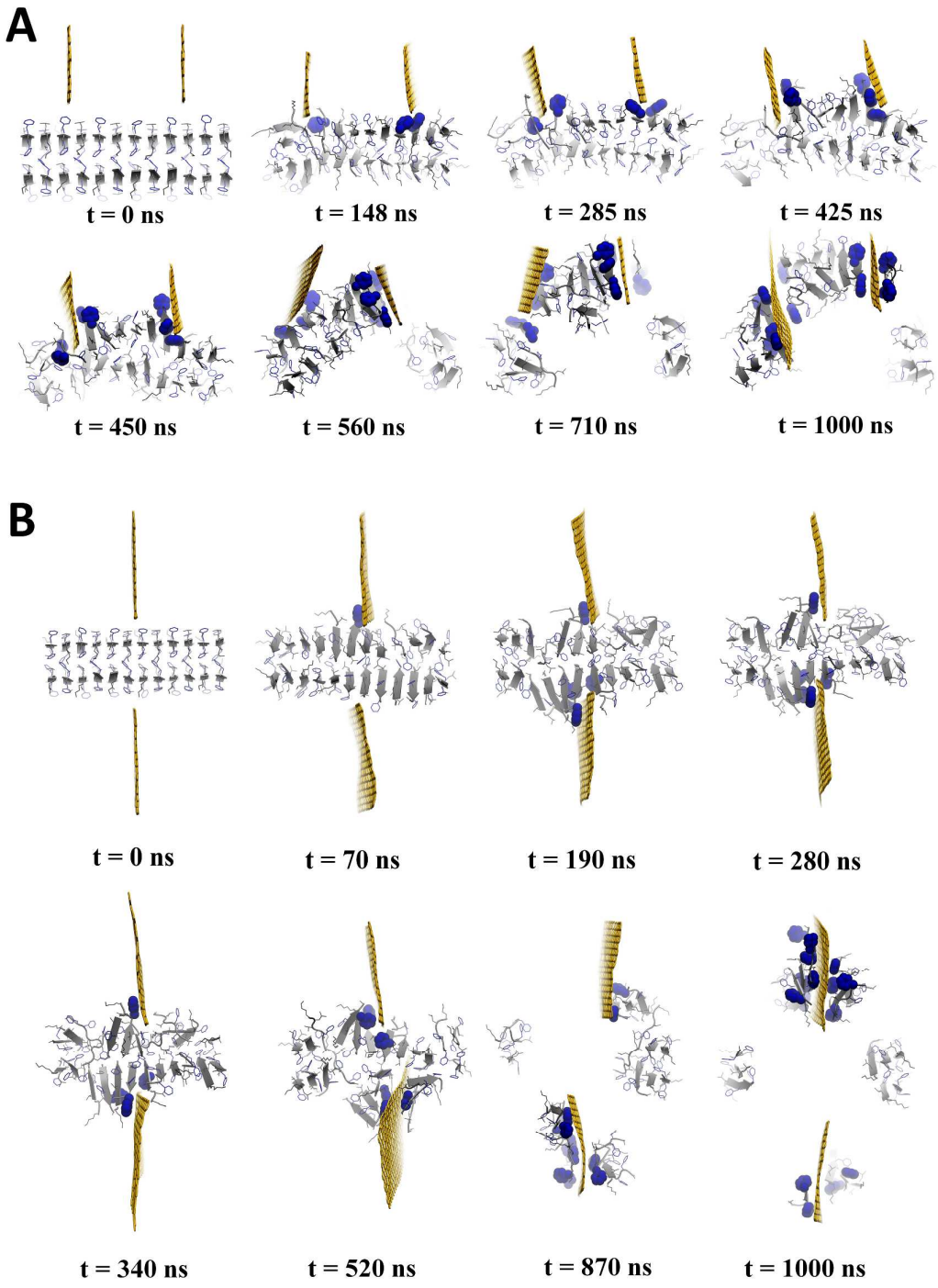

Fig .1

Fig. 2

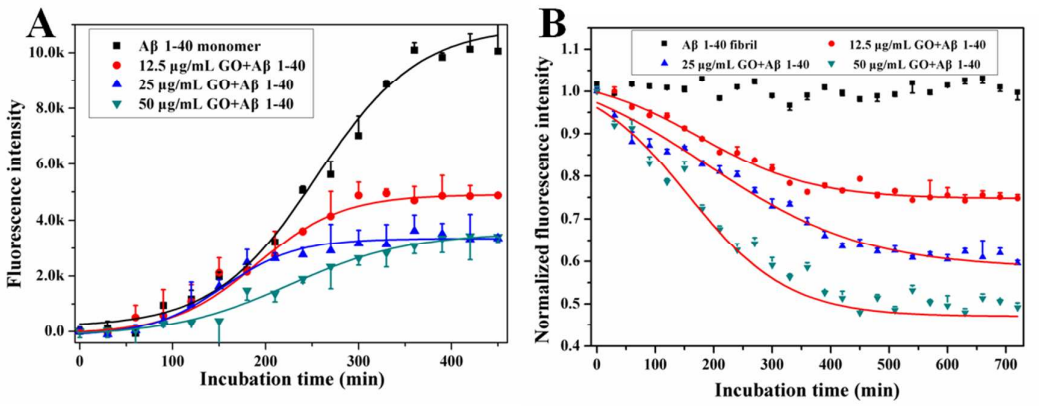

Fig. 3

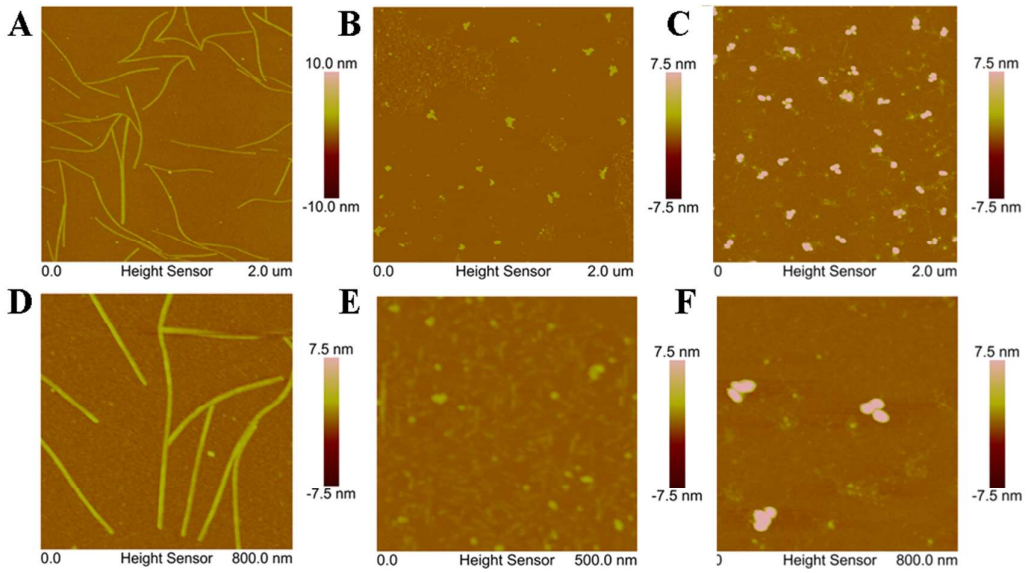

Fig. 4

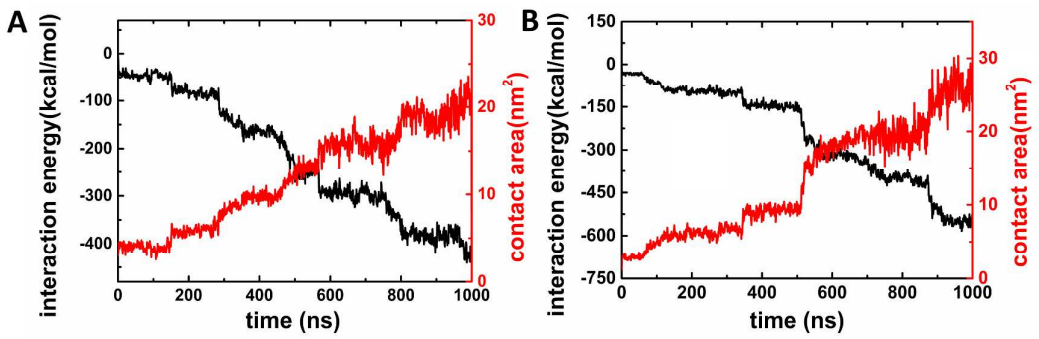

Fig. 5

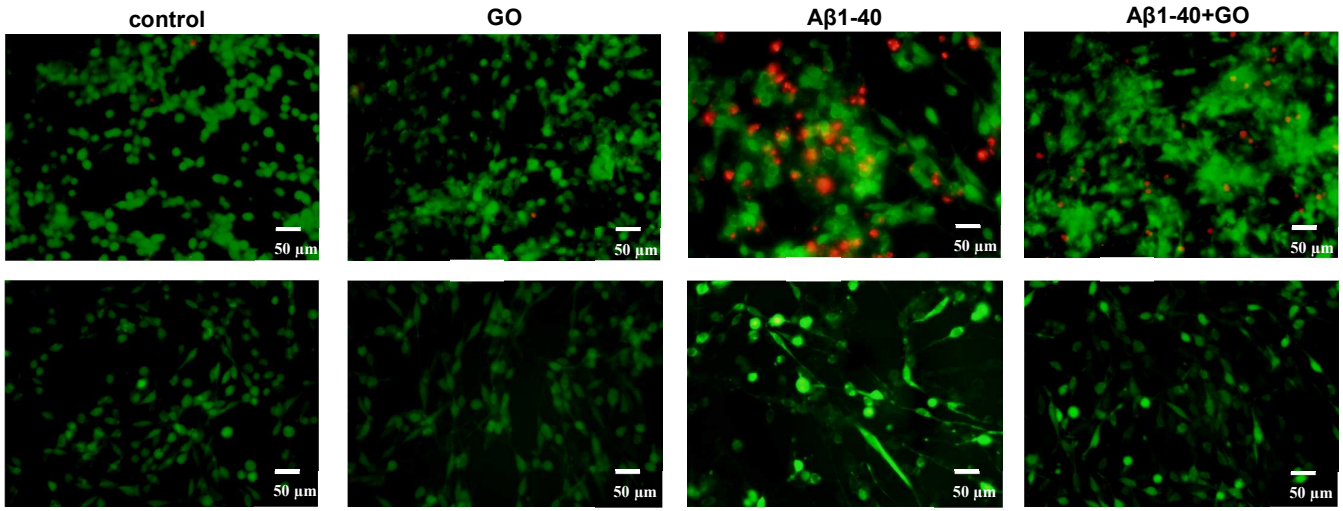

Fig. 6